Astron. Astrophys. 317, 776–785 (1997)

ASTRONOMY AND ASTROPHYSICS

EUV Emission from RS Canum Venaticorum binaries

C.K. Mitrou[1,2], **M. Mathioudakis**[1,3], **J.G. Doyle**[1], **and E. Antonopoulou**[2]

[1] Armagh Observatory, College Hill, Armagh BT61 9DG, N. Ireland (email: kam@star.arm.ac.uk & mm@star.arm.ac.uk & jgd@star.arm.ac.uk)
[2] Sect. of Astrophysics, Astronomy and Mechanics, Dept. of Physics, Univ. of Athens, Athens 15783, Greece (email: kam@rigel.da.uoa.gr & eantonop@rigel.da.uoa.gr)
[3] current: Dept. of Pure & Applied Phys, Queens University Belfast, Belfast BT7 1NN, N. Ireland (email: M.Mathioudakis@Queens-Belfast.AC.UK)

Received 2 November 1995 / Accepted 30 May 1996

Abstract. We performed a study of 104 RS CVn systems in the extreme ultraviolet (EUV) using the all–sky survey data obtained by the Extreme Ultraviolet Explorer (EUVE). The present sample includes several new RS CVn detections; 11 more than in the published EUVE catalogs, and 8 more than in the ROSAT Wide Field Camera catalog. The ratio of detections to non–detections remained constant throughout the sky, implying that our detections are not limited by the exposure time but are most likely limited by absorption from the interstellar medium. A general trend of increasing Lex/B (50–180Å) flux with decreasing rotational period is clear. The dwarf systems exhibit a leveling-off for the faster rotators. In contrast, the evolved systems exhibit no such effect. For the RS CVn systems the losses in the EUV represent a smaller fraction of the coronal radiative losses, as compared to active late–type dwarfs.

Key words: binaries: close – ultraviole: stars – stars: coronal – stars: activity

1. Introduction

The RS Canum Venaticorum binaries typically consist of a late–type (G or K) chromospherically active and usually evolved star, forced into faster rotation than its age and evolutionary status implies by the presence of a companion which may (or may not) be active as well. The phenomena associated with these stars originate from high magnetic activity due to very active dynamos operating as a result of deep convective zones and fast rotation. The study of this activity in the UV, EUV and X–ray part of the spectrum has become possible with the launch of the IUE, and subsequently EXOSAT, Einstein, HST, ROSAT, and EUVE satellites. The RS CVn systems occupy a prominent position among the late–type stars insofar as they exhibit the highest luminosities in the X–ray part of the spectrum (Dempsey et al. 1993b), indicating that they possess very active coronae. As a result of their detectability, there have been many papers dealing specifically with their behaviour in the X–ray and more recently, the EUV. Among these studies, the most relevant to this present work are the ROSAT–based papers by Pye et al. (1995) and Dempsey et al. (1993b).

The EUV region is an important part of the electromagnetic spectrum providing numerous hot coronal lines, some of which are sensitive to electron density variations. However, its overall contribution to the radiative losses from the stellar atmosphere is largely unknown. In the present study, we use broad-band data collected with the EUVE satellite (Bowyer et al. 1994) during an all–sky survey lasting six months up to July 1993. The survey was conducted in four bands, namely Lex/B (50–180Å), Al/Ti/C (160–240Å), Ti/Sb/Al (345–605Å) and Sn/SiO (500–740Å), with peak sensitivities at approximately 100, 180, 400 and 550Å respectively. The primary objectives of our work are to: (i) identify new RS CVn systems with detectable EUV emission, (ii) determine the EUV activity levels of all RS CVn binaries and (iii) investigate the validity of correlations between the EUV radiative losses and other parameters. Our findings are compared to previous studies based on ROSAT data.

2. Observations and data reduction

2.1. Count rates

The sample of stars investigated consists of the 104 systems classified as RS CVn-type binaries in the Strassmeier et al. (1988) Catalog of Chromospherically Active Binary Stars (CCABS). Their distribution in the sky is shown on an Aitoff projection in ecliptic coordinates in Fig. 1, with the detections depicted as filled circles. Due to the geometry of the EUVE survey, the ecliptic poles received maximum exposure time with minimum exposure time at the ecliptic equator. Note however, that the ratio of detections to non–detections remains constant throughout the sky, implying that our detections are not limited by the exposure time, but are more likely limited by absorption from the interstellar medium.

Send offprint requests to: C.K. Mitrou

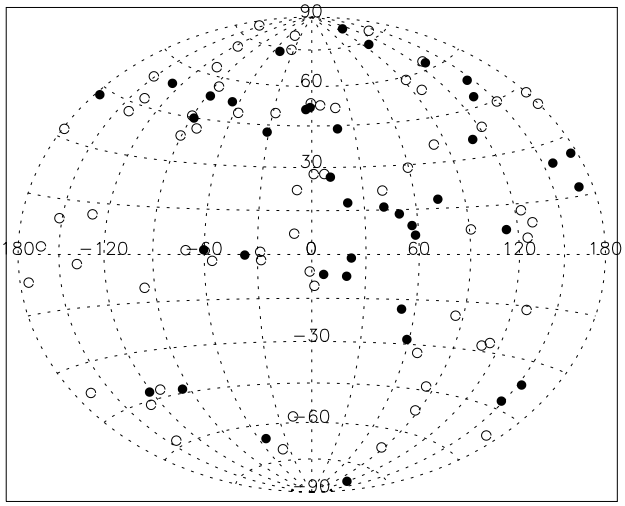

Fig. 1. The RS CVn systems in Ecliptic coordinates (circles). Filled symbols represent the sources with a 3σ detection.

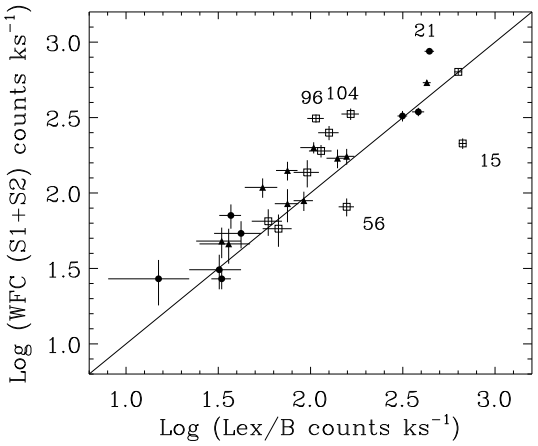

Fig. 2. Our Lex/B count rates against the ROSAT WFC (S1+S2) values; the symbols are as follows. Circles: systems comprising of giant stars. Squares: subgiants. Triangles: dwarfs. The source index numbers are explained in Table 1.

The source count rates were determined by applying a maximum likelihood method to a group of photon events collected from a circular area with a radius of 24 arc minutes centered on the optical position of the source. Here we examine the Lex/B and the Al/Ti/C bands. In both filters we consider significant all the detections with a maximum likelihood significance greater than 9 corresponding to 3σ. Detector background dominates the Lex/B background, while the most important source of background in Al/Ti/C is due to the HeII 304Å geocoronal emission. For weak detections the main source of uncertainty in the count rates comes from counting statistics, whereas for stronger detections the principal source of uncertainty is introduced by vignetting effects.

To obtain our count rates we have used the full EUVE sky survey dataset, the latest vignetting maps, and for the derivation of fluxes as described in Sect. 3, the most up–to–date effective areas of the EUVE photometers. The results are shown in Table 1 for the valid ($\geq 3\sigma$) detections. For the non–detections, 3σ upper limits are given in Table 2. We found 38 detections in the Lex/B, and 11 in the Al/Ti/C band. For the detected sources the coincidence between the EUVE and optical positions is better than $60''$. If a discrepancy of more than $60''$ between the two positions was found, then the source was rejected as spurious and an upper limit was determined. At this point we emphasize that, given the size of our sample and based on a random sample test, (see Fruscione (1996) for a detailed description), we would expect 2 spurious detections in each band at the 3σ level.

The initial EUVE Bright Source List (BSL) by Malina et al. (1994) lists 27 RS CVn detections in the Lex/B band and 4 in the Al/Ti/C. The subsequent EUVE Bright Source Catalog (BSC) by Bowyer et al. (1994) includes 21 Lex/B and 7 Al/Ti/C detections in the main table. The remaining six BSL detections did not meet the BSC's criteria for inclusion in the main table and were listed separately. The Al/Ti/C counts quoted in the BSC for 096 = AR Lac and 104 = II Peg were obtained by Patterer et al. (1993), when using the two systems as EUVE in–flight calibration targets. Our detections (Table 1) include all of BSC and BSL's detections in both bands, except for 104 = II Peg and 096 = AR Lac in the Al/Ti/C band where we only quote upper limits, that are 2.4 and 7.4 times higher respectively than the Patterer et al. (1993) values. The RS CVn systems 027 = TZ Pic and 094 = RT Lac were detected only in Al/Ti/C. We shall return to these objects in Sect. 5.

2.2. Comparison to the ROSAT results

During 1990–1991 the Wide Field Camera (WFC) on board the ROSAT satellite conducted an all–sky survey at EUV wavelengths, using two broadband filters, namely S1 and S2. Filter S1 covered the range 60-140Å, and S2 the range 112-200Å. The range covered by S1+S2 is similar to the EUVE Lex/B band (50–180Å); note however the overlap of S1 and S2 between 112 and 140Å. The WFC results can be found in Pounds et al. (1993), Bright Source Catalogue, and more recently, after an improved reprocessing of the database, in the 2RE Source Catalogue (2RESC) by Pye et al. (1995).

Out of our sample, 2RESC identifies 33 significant detections. The systems not detected by the WFC are flagged in Table 1. With the exception of the three systems: 022 = TW Lep, 057 = HD 119285 and 100 = SZ Psc (flagged in Table 2) that were detected only in the S1 filter of the WFC, all the remaining objects were also detected by EUVE in the Lex/B band. The count rates we found for our sample are in agreement with the WFC count rates, ranging between 50 and 100% of the S1+S2 value. Given the slightly different spectral range, the differences in effective areas, the overlap between S1 and S2 and the possible variability of the sources, we consider this as reasonable agreement. Strong emission lines of Fe ions are present in the spectra of RS CVn stars in the overlapping wavelengths, e.g. Fe XXIII/Fe XX 132.85Å, Fe XXII 135.78Å, Fe XXII 117.17Å and Fe XXI 128.73Å (see Fig. 4 later). The counts for 021 = Capella and 104 = II Peg, two strong detec-

Table 1. The 104 RS CVn systems in the Extreme Ultraviolet. This table contains the significant (i.e. $\geq 3\sigma$) detections in Lex/B and/or Al/Ti/C. For the non-detections (3σ) upper limits (UL) are given. Columns 1 & 2 contain an index number for each system and its most common name. The systems are numbered in increasing RA order. Column 3 gives the distance in parsec followed by the corresponding hydrogen column density to the source in column 4. In column 5 we give the CIV observed flux (our own reduction of IUE spectra) in units of 10^{-13}erg cm^{-2} s^{-1}. Columns 6, 7, and 8 contain the data for the Lex/B passband in the following order: the count rate and the 1σ statistical error in counts ks^{-1}, its significance (σ), and the broadband flux in units of 10^{-12}erg cm^{-2} s^{-1} assuming a coronal temperature model of $\log T = 6.8$. In columns 9, 10 and 11 the corresponding values for the Al/Ti/C filter are given in the same units.

SOURCE NAME		Dist.	$\log N_{\rm H}$	$f_{\rm CIV}$	Lex/B			Al/Ti/C		
(Index)	Common or HD	(pc)	(cm^{-2})	(10^{-13})	ct ks^{-1}	σ	$f_{6.8}$	ct ks^{-1}	σ	$f_{6.8}$
003	HD 3196	21	18.79	2.8	36±11	5	1.2	59±20	4	6.3
004	ζ And	31	19.81	18.1	37 ± 5	10	7.2	16 ± 5	3	11.8
005	CF Tuc	54	19.84	4.2	67 ± 12	8	14.4	30 UL	-	22.9
006	UV Psc[a]	125	19.09	-	19 ± 7	3	0.8	56 UL	-	21.7
008	HD 8358	60	18.73	1.4	33 ± 9	5	1.1	58 UL	-	5.5
009	AR Psc	17	18.73	6.4	157 ± 16	17	5.1	40 ± 13	4	3.8
011	6 Tri[a]	75	19.65	8.5	24 ± 9	4	3.1	38 UL	-	23.3
013	VY Ari	21	19.35	9.2	126 ± 16	13	6.4	80 UL	-	31.5
015	UX Ari	50	19.09	15.5	668 ± 32	43	28.4	99 ± 20	7	20.9
016	HR 1099	36	17.96	38.1	632 ± 31	39	17.0	84 UL	-	3.8
017	HD 22403	55	19.09	6.5	104 ± 16	10	4.4	40 UL	-	8.7
018	EI Eri	75	19.46	7.9	114 ± 16	12	8.5	74 UL	-	34.5
021	Capella	13	18.73	390.0	441 ± 26	33	14.4	144 ± 19	12	13.7
027	TZ Pic	60	17.96	1.1	12 UL	-	-	15 ± 5	3	0.7
032	σ Gem	59	18.85	35.2	384 ± 29	25	13.4	52 ± 21	3	6.4
033	AE Lyn[a]	38	18.28	2.6	18 ± 6	4	0.5	24 UL	-	1.3
037	TY Pyx	55	19.06	4.5	59 ± 11	9	2.4	70 UL	-	14.0
040	IL Hya	138	18.99	4.0	32 ± 10	4	1.2	44 UL	-	7.5
042	DM UMa	130	19.49	1.0	15 ± 7	3	1.2	44 UL	-	22.4
043	ξ UMa	7.9	18.00	8.3	140 ± 18	13	3.8	88 UL	-	4.0
047	DQ Leo	36	19.39	-	42 ± 12	5	2.7	76 UL	-	32.3
049	DK Dra[a]	130	19.60	4.6	29 ± 8	5	3.0	36 UL	-	20.8
051	IL Com	86	19.28	2.1	24 ± 9	4	1.3	44 UL	-	15.0
056	BH CVn	53	18.58	17.2	157 ± 15	18	4.8	44 ± 15	4	3.3
059	HD 127535	63	18.68	1.2	20 ± 10	3	0.7	96 UL	-	8.6
067	TZ CrB	21	18.56	18.1	472 ± 21	44	14.3	90 ± 15	8	6.6
069	ϵ UMi[a]	71	19.44	8.58	15 ± 4	5	1.1	12 UL	-	5.5
071	V824 Ara	39	18.68	7.1	96 ± 15	10	3.1	54 UL	-	4.8
074	DR Dra	88	19.46	5.1	33 ± 4	12	2.4	24 UL	-	11.1
077	V772 Her	42	19.18	3.2	75 ± 11	11	3.5	42 UL	-	11.3
078	V815 Her	31	19.17	4.5	75 ± 10	12	3.5	46 UL	-	12.1
082	V478 Lyr	26	19.12	2.7	92 ± 11	14	4.0	48 UL	-	11.1
083	HR 7275[a]	90	19.68	6.3	17 ± 5	5	2.2	28 UL	-	17.9
087	HD 190540[a]	110	19.65	-	26 ± 11	3	3.1	56 UL	-	34.4
090	ER Vul	46	19.32	4.0	55 ± 11	7	3.2	78 UL	-	28.9
093	42 Cap[a]	34	18.60	4.3	41 ± 11	6	1.3	50 UL	-	3.9
094	RT Lac[b]	205	20.52	1.1	18 UL	-	-	43 ± 16	3	92.5
096	AR Lac	47	18.73	13.9	107 ± 11	16	3.5	52 UL	-	5.1
102	λ And	24	18.73	30.2	315 ± 19	31	10.2	36 ± 11	4	3.5
104	II Peg	29	18.73	9.1	165 ± 18	17	5.4	72 UL	-	7.0

[a] Not detected by ROSAT's WFC

[b] Not detected by ROSAT's WFC, but our Al/Ti/C detection may be spurious

tions, are found at the lower end of this range ($\approx 50\%$). In Fig. 2 we show our count rates plotted against the rates quoted in the 2RESC.

Notable differences from the ROSAT WFC values are derived for 015 = UX Ari, 056 = BH CVn, 074 = DR Dra, and 096 = AR Lac. Systems UX Ari and BH CVn have EUVE count rates higher by factors of 2 and 3 times respectively. An initial timing analysis of the EUVE data however, showed that the EUVE counts were affected by flaring. DR Dra has 20% higher EUVE counts. It comprises of a K0-2 giant and a hot white dwarf companion (of $T = 30,000$ K according to Fekel et al. 1993), so the WD's contribution in the EUV might explain this discrepancy. The AR Lac counts though, are at 35% of the ROSAT value. Patterer at al. (1993), report similar find-

Table 2. The RS CVn systems in the Extreme Ultraviolet. This table contains the systems that are not acceptable detections ($< 3\sigma$), in any of the two filters. Columns 1 & 2 contain an index number for each system and its most common name. The systems are numbered in increasing RA order. Column 3 gives the distance in parsec followed by the hydrogen column density to the source in column 4. Columns 5 and 6 contain the data for the Lex/B passband, in the following order: the 3σ Upper Limit (UL) and the corresponding flux upper limit in units of 10^{-12}erg cm^{-2} s^{-1} for a temperature model at $\log T$ = 6.8. In columns 7 and 8 similarly we give the Al/Ti/C filter 3σ UL count rate, and the corresponding flux value for $\log T$ = 6.8 in units of 10^{-11}erg cm^{-2} s^{-1}.

SOURCE NAME		Dist.	log $N_{\rm H}$	Lex/B UL		Al/Ti/C UL	
(Index)	Common or HD	(pc)	(cm^{-2})	ct ks^{-1}	$f_{6.8}$	ct ks^{-1}	$f_{6.8}$
001	33 Psc	111	18.90	32	1.2	66	0.9
002	BD Cet	71	18.90	30	1.1	82	1.1
007	HD 8435	100	19.62	20	2.2	56	3.4
010	HD 12545	310	20.68	16	71.2	42	12.4
012	HD 14643	77	20.00	10	3.8	32	3.1
014	LX Per	130	20.79	32	197.0	22	7.8
019	RZ Eri	143	19.84	30	6.4	38	2.9
020	12 Cam	134	20.60	36	127.0	40	9.8
022	TW Lep[a]	220	19.65	28	3.3	50	3.1
023	HD 37824	164	20.19	44	37.6	50	6.3
024	HD 39576	85	18.21	28	0.8	48	0.2
025	SZ Pic	30	17.96	22	0.6	20	0.1
026	CQ Aur	220	20.76	28	150.0	42	14.2
028	SV Cam	74	19.49	28	2.2	12	0.6
029	VV Mon	380	20.02	16	6.9	30	3.0
030	SS Cam	255	20.31	10	13.6	16	2.4
031	AR Mon	525	20.12	32	20.6	52	5.8
034	GK Hya	220	19.99	32	12.1	78	7.2
035	RU Cnc	300	20.05	34	16.4	50	5.0
036	RZ Cnc	395	20.05	24	11.6	52	5.3
038	WY Cnc	160	19.85	22	4.9	46	3.6
039	XY UMa	100	19.28	26	1.4	24	0.8
041	IN Vel	500	20.13	30	20.1	34	3.9
044	HD 101309	62	17.79	16	0.4	34	0.1
045	HD 101379	140	20.16	24	18.3	36	4.3
046	RW UMa	150	19.72	16	2.3	34	2.3
048	HU Vir	220	19.40	26	1.7	52	2.3
050	AS Dra	29	17.40	30	0.8	28	0.1
052	UX Com	350	19.91	38	10.6	34	2.8
053	HD 113816	165	20.00	18	7.1	38	3.6
054	RS CVn	180	19.80	42	7.9	42	3.0
055	BM CVn	250	19.89	40	10.3	34	2.8
057	HD 119285[a]	80	19.63	58	6.5	148	9.0
058	BH Vir	166	20.02	16	6.9	72	7.0
060	RV Lib	270	20.53	40	115.3	34	7.4
061	SS Boo	220	19.99	20	7.6	32	3.0
062	UV CrB	230	19.92	34	9.7	42	3.5
063	GX Lib	219	20.37	30	49.6	68	11.4
064	LS TrA	54	18.68	26	0.8	14	0.1
065	RT CrB	360	19.93	18	5.4	56	4.8
066	RS UMi	350	20.03	6	2.8	24	2.3
068	WW Dra	180	19.98	12	4.4	12	1.1
070	V792 Her	310	19.98	14	4.9	24	2.3
072	HR 6469	69	19.22	28	1.4	36	1.1
073	HD 158393	400	20.85	30	213.2	52	20.7
075	Z Her	100	20.37	22	37.6	50	8.4
076	MM Her	190	19.57	14	1.3	64	3.6
079	PW Her	285	19.90	12	3.3	36	3.0
080	AW Her	315	20.31	12	16.9	50	7.5
081	o Dra	67	19.21	12	0.6	20	0.6
084	HD 181809	210	20.59	46	161.0	60	14.8
085	HR 7428	302	20.80	20	118.7	20	7.6
086	HD 185151	390	20.50	20	52.9	42	8.6
088	AT Cap	99	20.20	66	58.8	38	4.8
089	CG Cyg	63	19.59	22	2.2	62	3.6
091	AS Cap	93	20.19	24	20.3	80	10.0
092	AD Cap	250	20.50	22	56.3	40	8.2
095	HK Lac	150	20.48	20	50.0	32	6.4
097	V350 Lac	69	19.44	22	1.6	30	1.4
098	IM Peg	50	19.40	56	3.7	54	2.3
099	RT And	95	19.97	12	4.4	20	1.8
100	SZ Psc[a]	125	19.92	54	15.7	34	2.9
101	EZ Peg	83	19.75	38	5.7	84	5.8
103	KT Peg	25	18.73	36	1.2	94	0.9

[a] Detected by ROSAT's WFC S1 band

ings when using AR Lac as an EUVE in–flight calibration target, and attributed this deviation to long–term EUV variability of the system. On the other hand, McGale et al. (1995), who performed a timing analysis of the ROSAT all–sky survey data, found temporal variability for this system, and suggested the possibility of a flare.

Apart from the WFC, one more instrument on board ROSAT, the Position Sensitive Proportional Counter (PSPC) performed an all–sky survey. The PSPC covers energies between 0.1 and 4 keV (or equivalently, the spectral range 5–124Å). A thorough study of a large sample of RS CVn stars (112 detections out of 136 observed) is presented in Dempsey et al. (1993b). All of our detections (as well as all the WFC detections) were detected by the PSPC. In Fig. 3 we have plotted the Lex/B against the PSPC count rates. The strikingly deviating systems are the flaring 015 = UX Ari (see previous paragraph) and 087 = HD190540, which appears overluminous in the EUV (see also Sect. 4).

3. Derivation of fluxes

In order to derive fluxes from the count rates, the neutral hydrogen column density along the line of sight ($N_{\rm H}$) has to be determined, and a specific coronal model adopted. In the present study, only the Lex/B (50–180Å) and Al/Ti/C (160–240Å) passbands are considered.

3.1. Interstellar medium attenuation

We determined the values for the hydrogen column densities by using a model of the interstellar medium developed by Jelinsky

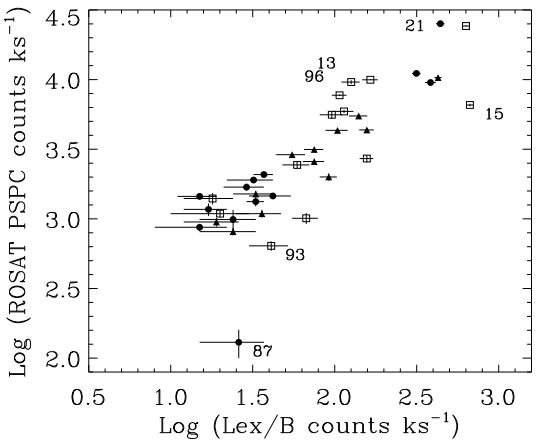

Fig. 3. Our Lex/B count rates against the ROSAT PSPC values; the symbols are as in Fig. 2

& Fruscione (1996). In order to estimate the amount of hydrogen in any given direction and distance, this method performs a three–dimensional interpolation on a large database of HI column densities (Fruscione et al. 1994). The ISM attenuation was calculated using the hydrogen and helium photoionization cross sections compiled by Rumph et al. (1994). A ratio of HeI/HI = 0.1 was used. However, since the distribution of neutral hydrogen in the interstellar medium (ISM) is extremely irregular and given the fact that the software employs an interpolation, the accuracy of the method relies on the number of stars with directly measured $N_{\rm H}$ used in the fit.

Dempsey et al. (1993a), in their paper on ROSAT data, quote hydrogen column densities for some of the EUVE detections. Comparing their column densities to the ones obtained with the method described above, we find that most are in agreement in the sense that they yield fluxes within 50%. For system 015 = UX Ari, the Jelinsky & Fruscione (1996) method provided us with an unrealistically high value for $N_{\rm H}$ ($\log N_{\rm H}$ = 20.33). For this object we adopted a $\log N_{\rm H}$ = 19.09 from Dempsey et al. (1993a).

The distances to our objects come into the picture twice. Initially, they affect the value for $N_{\rm H}$ and thus the conversion of count rates into observed fluxes, and subsequently, when converting the observed fluxes to surface fluxes or luminosities. Direct parallax measurements exist for only few of our stars and unfortunately, for many of our targets, we have encountered in the literature substantial differences concerning this parameter. We have used, as a rule, the distances and radii quoted in the second CCABS (Strassmeier et al. 1993), except for a few systems mentioned in Sect. 4.

The analysis of spectroscopic observations of RS CVn systems to date (Dupree et al. 1993, Mitrou et al. 1996) have shown that, in the spectral range covered by the Lex/B filter, a significant fraction of the total counts correspond to emission lines of highly ionised Fe which are formed between $\log T$ = 6.5 and 7.2. The hydrogen column densities used in the present study (see Tables 1 & 2) extend over two orders of magnitude. So, we examined the dependence of the conversion factor (from counts per second to flux units) on the assumed temperature model, and on the adopted $N_{\rm H}$ value. This is presented in Table 3 for the Lex/B and Al/Ti/C filters.

Table 3. Effects of assumed temperature model and hydrogen column density on obtaining fluxes from count rates. The fluxes for the one–temperature models correspond to a count rate of 1 ct s^{-1} and are given in units of 10^{-11} erg cm^{-2} s^{-1}.

Log	Lex/B filter			Al/Ti/C filter		
$N_{\rm H}$	$f_{6.5}$	$f_{6.8}$	$f_{7.0}$	$f_{6.5}$	$f_{6.8}$	$f_{7.0}$
17.50	3.81	2.62	2.85	4.50	3.90	3.82
18.00	3.97	2.70	2.95	5.50	4.50	4.34
18.30	4.20	2.83	3.15	6.98	5.50	5.17
18.60	4.65	3.07	3.56	10.60	7.70	7.00
18.70	4.91	3.20	3.78	12.80	9.02	8.27
18.90	5.59	3.60	4.47	20.74	13.34	12.22
19.10	6.67	4.30	5.78	39.00	21.70	20.12
19.25	7.90	5.17	7.59	66.36	31.65	29.97
19.35	9.00	6.04	9.54	92.79	39.42	38.26
19.50	11.27	8.08	14.51	136.60	50.80	51.80
19.65	14.75	11.76	24.31	172.70	61.40	65.91
19.88	24.72	24.83	60.24	224.20	80.70	90.77
20.00	34.40	39.44	98.01	261.60	94.50	107.04
20.20	65.91	88.89	214.30	357.00	126.70	142.91
20.35	114.38	157.93	371.60	466.70	160.80	181.73
20.50	199.12	262.29	596.35	625.20	208.00	234.80
20.65	330.56	409.69	896.30	850.50	274.50	311.30

Columns 2, 3 and 4 give the Lex/B fluxes resulting from the use of single–temperature models at $\log T$ = 6.5, 6.8, and 7.0 in units of 10^{-11} erg cm^{-2} s^{-1} per ct s^{-1}, for various values of $\log N_{\rm H}$. The values in Tables 1, 2 & 3 were determined using the Monsignori–Fossi & Landini (1994) line emissivities.

3.2. Single–temperature coronal model

We note that for $\log N_{\rm H}$ between 17.50 and 19.10 cm^{-2}, the choice between the 6.5 and the 6.8 models affects the resultant Lex/B flux within 50%, while the difference between the 6.8 & 7.0 models is $\approx$ 25%. At higher column densities though (e.g. $\log N_{\rm H} \approx 20$ cm^{-2}), the reverse is true: little difference exists between the two lower temperature models, but a factor of two difference in the resultant Lex/B flux occurs between the higher temperature models. For the Al/Ti/C filter fluxes (columns 5, 6 and 7) there is negligible difference between the 6.8 and 7.0 models. If we assume the model at 6.5 though, we obtain significantly higher fluxes, indicating a strong dependence on lower temperatures.

Considering each temperature model separately, we note that, for $\log N_{\rm H}$ below 18.60 cm^{-2}, the conversion factor is relatively insensitive to the column density value adopted, and remains within 100% for both filters. For higher column densities though, the picture changes dramatically as the resultant fluxes increase very sharply with increasing $\log N_{\rm H}$. In Fig. 4, we present sample spectra for the coronal models considered. These spectra have been folded through the EUVE Lex/B and Al/Ti/C effective areas. Fig. 5 shows graphically a summary

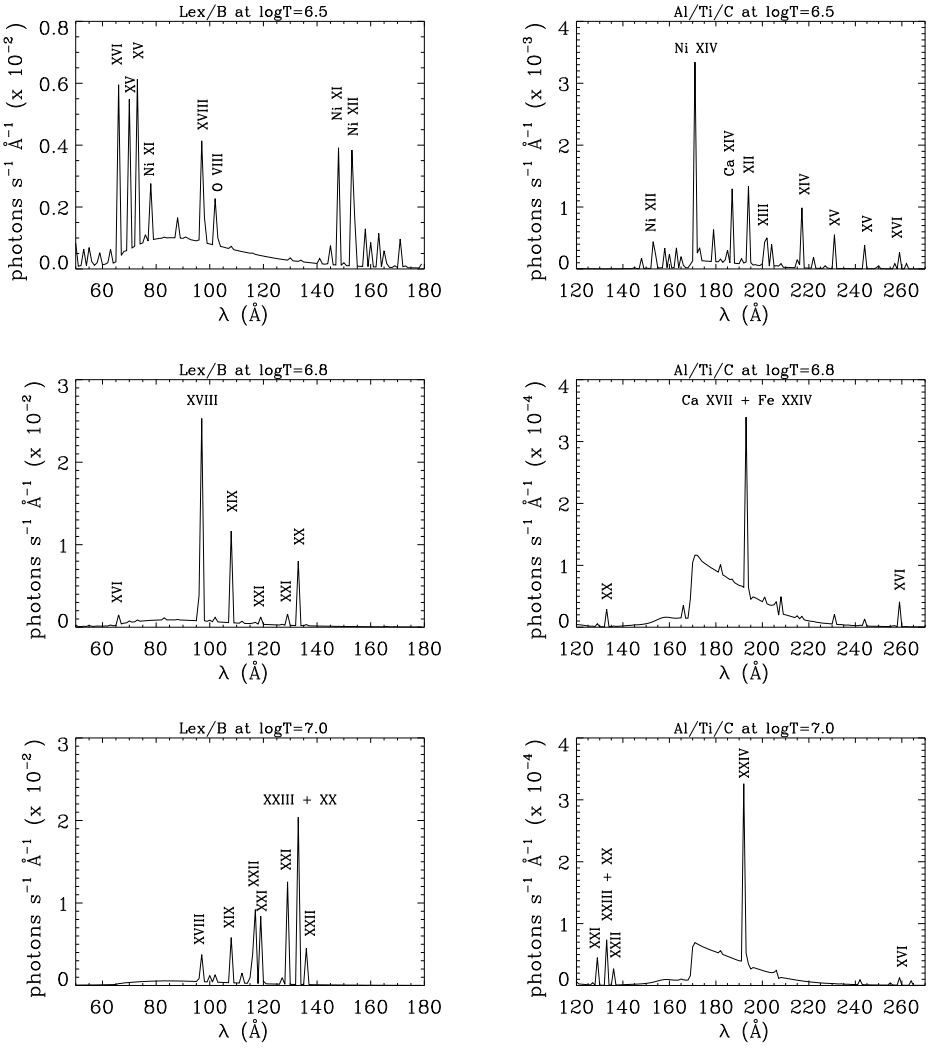

Fig. 4. Plasma models for $\log T$ = 6.5, 6.8 & 7.0 folded through the EUVE Lex/B and Al/Ti/C effective areas. The models were determined using the Monsignori-Fossi & Landini (1994) line emissivities with $\log N_{\rm H}$ = 18.70 cm^{-2} at a distance of 30pc.

of the conversion from count rates (ct s^{-1}) to observed fluxes (10^{-11} erg cm^{-2} s^{-1}), plotted against hydrogen column density for the three temperature models (i.e. $\log T$ = 6.5, 6.8 and 7.0).

The Lex/B filter spectral range roughly coincides with the range (80–160Å) covered by the short wavelength spectrometer on board EUVE. To test the quality/validity of the single–temperature assumption, we have analyzed the available EUV spectra for seven of our detections (i.e. HR 1099, Capella, σ Gem, ξ UMa, AR Lac, λ And and II Peg), and compared the observed integrated flux from these spectra to the flux predicted by the single–temperature model at $\log T$ = 6.8. The observed flux of 102 = λ And is equal to 62% of the predicted value, while for the remaining six objects the agreement is better than 25%. Taking into consideration the errors from counting statistics, (for these objects, between 5 and 10%), possible flaring incidents and the general variability of the systems, the single–temperature approximation gives fluxes good to $\approx$ 25%. Hence, in our tables and figures throughout the paper, we used as flux density the value resulting from the adoption of a $\log T$ = 6.8 coronal model.

4. Results & Discussion

In Fig. 6a we plot the EUVE Lex/B fractional luminosity against the X–ray data from Dempsey et al. (1993b). In almost every case these authors used the distances quoted in CCABS to obtain luminosities, so the distances are the same as ours. The only exceptions were the distances to systems 009 = AR Psc, 011 = 6 Tri, 040 = IL Hya, and 083 = HR 7275. For systems AR Psc, 6 Tri and IL Hya Dempsey et al. (1993b) use distances of 70, 14.7 and 138 pc respectively, while CCABS quotes 17, 75 and 263 pc.

For the first two objects, we modified the given X–ray luminosity and flux to correspond to the CCABS distance, and for IL Hya we adopted their value. For object HR 7275, Dempsey et al. (1993b) use a distance of 48 pc, and the CCABS quotes 250 pc. CCABS mentions explicitly that, the distance of 48 pc is obviously wrong, but on the other hand the 250 pc distance yielded unrealistically high value for $L_{\rm Lex}$. Therefore, we used the value given by Slee et al. (1987), and Drake et al. (1989), of 90 pc (a distance of 250pc with the corresponding higher $N_{\rm H}$, would produce a flux 200 times greater). Also for system

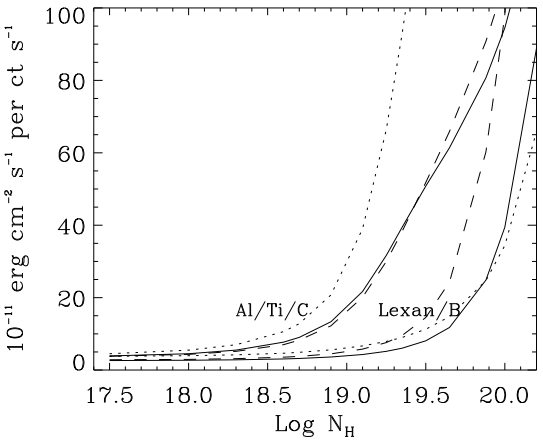

Fig. 5. Conversion factors from counts per second into flux (in units of 10^{-11} erg cm^{-2} s^{-1}) for various values of log N_H. Linestyles are as follows: *Dotted*: Lex/B & Al/Ti/C for log T = 6.5. *Solid*: Lex/B & Al/Ti/C for log T = 6.8. *Dashed*: Lex/B & Al/Ti/C for log T = 7.0.

087 = HD190540 we adopted a distance of 110 pc from Drake et al. (1989), instead of the 340 pc value quoted in CCABS. This latter distance would yield very high N_H and consequently an even higher flux value. But even at the lower distance and hence lower N_H, the system is found to be overluminous in the Lex/B band (Fig. 6a).

The apparent bolometric luminosities were obtained from Basri et al. (1985); Drake et al (1989); Simon & Fekel (1987); Gurzadyan & Rustambekyan (1994)—objects 005 = CF Tuc, 006 = UV Psc and 059 = HD127535; and Katsova & Tsikoudi (1993)—object 013 = VY Ari. The CIV 1550Å data were the result of our own reduction using the IUEDR and DIPSO packages, which are available on the UK STARLINK network. When possible, the average value of several spectra were used. IUE SWP images do not exist for objects 006 = UV Psc, 087 = HD 190540, and the only existing spectrum of 047 = DQ Leo is saturated beyond 1450Å. For systems where both components have similar spectral type and luminosity class, in the plots, but *not* in Table 2, we attributed part of the apparent X–ray, EUVE and UV flux to both components in proportion to their radii. In the case of Capella we credited 90% of the flux to the hotter, smaller and faster rotating G1 III star (Ayres, 1984 and Simon & Fekel, 1987) and in the case of HR 1099 we considered the less active's component contribution as negligible (Dempsey et al. 1993b).

The systems deviating in Fig. 6a are 005 = CF Tuc, 015 = UX Ari, 042 = DM UMa and 087 = HD190540. A timing analysis of EUVE Lex/B data however, showed that the CF Tuc and UX Ari data are affected by flares. We have no explanation for the deviation of the giants DM UMa and HD190540. A search of the SIMBAD database for other sources near the expected positions of these objects, yielded negative results. The solid line in Fig. 6a was derived by using a least–squares linear fit to the data and corresponds to

$$\log(L_{\rm X-ray)}/L_{\rm bol}) = (1.00 \pm 0.07)\ \log(L_{\rm Lex}/L_{\rm bol}) + 0.81 \quad (1)$$

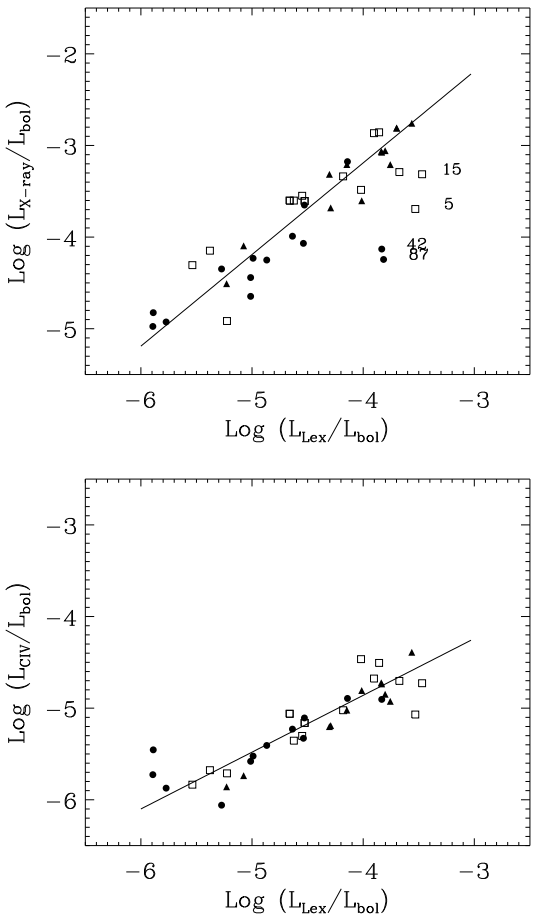

Fig. 6. a X–ray fractional luminosity versus the Lex/B, the straight line corresponds to Eq. (1); **b** The CIV fractional luminosity versus the Lex/B, the straight line corresponds to Eq. (2); symbols as in Fig. 2.

with a linear correlation coefficient of 0.93 if the obviously deviating systems are omitted. The mean slope was found by interchanging the independent variable.

This relation implies that the ROSAT PSPC X–ray luminosities for the RS CVn systems are roughly one order of magnitude greater than the Lex/B luminosities. Mathioudakis et al. (1995) examined the EUV activity of single dwarfs (types F–M) and found the two quantities to be of comparable magnitude (Mathioudakis et al. used X–ray fluxes obtained with Einstein, but these do not differ significantly from the ROSAT PSPC values). This only manifests the well–known fact that the coronae of the RS CVns are more active and at much higher temperatures than the coronae of single stars.

The correlation with CIV 1550Å can be seen in Fig. 6b, with the solid line representing the relation

$$\log(L_{\rm CIV}/L_{\rm bol}) = (0.62 \pm 0.04)\ \log(L_{\rm Lex}/L_{\rm bol}) - 2.38 \quad (2)$$

with a correlation coefficient of 0.93. Combining Eq. (1) & (2) we can derive that $\log(L_{\rm X-ray}/L_{\rm bol}) \propto 1.50\ \log(L_{\rm CIV}/L_{\rm bol})$. This is in very good agreement with the findings of Dempsey et al (1993) who, using a maximum likelihood method on a large

number (112) of RS Cvn systems' measurements by ROSAT's PSPC and CIV data from Simon & Fekel (1987), derived a slope of 1.40 ± 0.09. Similarly Fox et al. (1994), based on simultaneous ROSAT and IUE observations, determined an index of 1.24 ± 0.19 for this correlation. In Fig. 7 we show the corresponding surface fluxes, and again we note the particularly tight correlation (0.94) for the relation

$$\log F_{\rm CIV} = (0.78 \pm 0.05)\ \log F_{\rm Lex} + 0.86 \qquad (3)$$

The deviating systems are: 021 = Capella which seems to be underluminous in the EUV (see Sect. 2.2) and 005 = CF Tuc whose data have been contaminated by a flare.

The CIV versus Lex/B relation can also be used to check the upper limits of the RS CVn systems not detected by EUVE. For example, starting with the observed CIV flux for 100 = SZ Psc (Doyle et al. 1994), which is equal to 5×10^{-13} erg cm^{-2} s^{-1}, we derive using a conversion factor from observed to surface flux of 1.2×10^{18} and Eq. (3), a count rate of 13 ct ks^{-1}. This is consistent with the upper limit of 54 ct ks^{-1} given in Table 2.

Eq. (3) suggests that a source with a typical CIV surface flux of 10^5 erg cm^{-2} s^{-1} has a radiative flux in the 50 to 180Å region only a factor of 4 greater than the CIV flux. For sources with an order of magnitude higher CIV flux, the 50 to 180Å radiative losses are just one order of magnitude larger than in the CIV line alone. The relation from Doyle (1996) — originally developed for solar regions by Bruner & McWhirter (1988) — would imply that the spectral region covered by the Lex/B filter provides only a few percent of the total radiative losses from the plasma (the derived figure for the losses could be in error by a factor of two). This is in general agreement with the initial findings for λ And (Mitrou et al. 1996). For this system, multiplying the derived emission measure (EM) by the radiative loss function, it was determined that less than 10% of the total radiative losses originate from plasma at temperatures between $10^{5.2}$ and $10^{7.2}$ K. Capella has a similar percentage of losses in the same region (7%) while in the case of the Sun it is 21%, thus it appears that the losses in the 50 to 180Å region do not contribute significantly to the total radiative budget of the RS CVn systems. Instead the cooling is dominated by the losses from the chromosphere and lower transition region.

The rotation–activity relation in the EUV for the RS CVns is present but quite loose. As can be seen in Fig. 8, there is a general trend towards increasing surface flux with decreasing period. For comparison, we show in Fig. 9 $F_{\rm CIV}$ versus $\log P_{\rm rot}$. We have used photometric periods whenever there was a difference with the orbital period. The linear correlation coefficient between $\log F_{\rm Lex}$ and $\log P_{\rm rot}$ is 0.72, which improves to 0.77 if the strikingly deviating systems 087, 042 and 015 are omitted. Considering only the evolved stars, the linear correlation drops to 0.62, and if the above systems are once again omitted, it becomes 0.74. The optimal correlated results are achieved by introducing a minor gravity dependence of the form $\log F_{\rm Lex} \propto -0.84 \log P + 0.15\ \log g$. Then the coefficient becomes 0.78, so the improvement is not really significant. In Fig. 8 we plot all of our detections (giants, subgiants and dwarfs), and notice that only the dwarfs show an indication

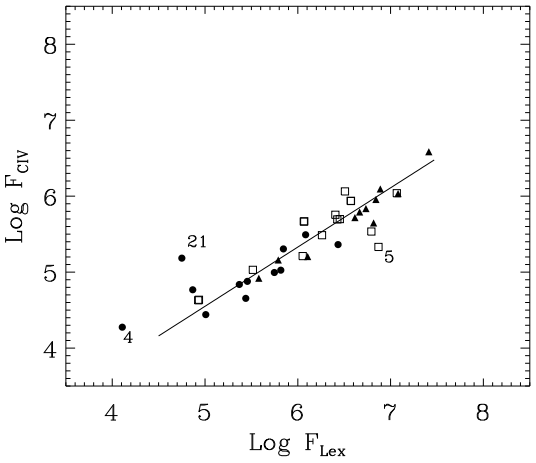

Fig. 7. The log–log diagram of surface Lex/B flux versus the CIV surface flux (in erg cm^{-2} s^{-1}). Symbols as in Fig. 2.

of 'saturation' in the Lex/B surface flux. The same applies for the CIV surface flux (Fig. 9).

5. Objects detected only at Al/Ti/C

Two of the objects in our sample, TZ Pic and RT Lac, were detected solely in the Al/Ti/C. In order to examine the consistency of the Al/Ti/C detections with the Lex/B upper limit we have run a number of one temperature model simulations. We have used the Al/Ti/C count rate, the $N_{\rm H}$ and the Monsignori-Fossi & Landini (1994) line emissivities to generate model spectra over the temperature range $5.2 \leq \log T \leq 7.6$ with a step of 0.1. We then folded the model spectra through the Lex/B effective areas and estimated the expected Lex/B count rate. In the case of TZ Pic we find that a coronal temperature of $\log T \leq 6.3$ is consistent with the Al/Ti/C detection and the Lex/B upper limit. Dempsey et al. (1993) list a PSPC count rate of 0.28 ± 0.04 ct s^{-1} for this source. Following a procedure similar to that described above, we find that the PSPC to Al/Ti/C flux ratio can be reproduced with a coronal temperature of $\log T = 6.2 - 6.3$. The interstellar hydrogen column density for TZ Pic is quite low. Furthermore the source lies in high ecliptic latitude and received an exposure time of 5200 sec in Al/Ti/C, which is significantly higher than the average EUVE survey exposure time of 1000 Sect. We therefore believe this detection to be real, despite of the fact that our modelling yielded a coronal temperature that is considered as extremely low for an RS CVn system. Note that a similar result was found for the low activity dwarf Gl 685 by Mathioudakis et al. (1995).

On the other hand RT Lac has a very high $N_{\rm H}$ and received an exposure time of 990 sec in the Al/Ti/C band. We have been unable to come up with a coronal model which would reproduce the correct Al/Ti/C count rate and at the same time be consistent with the Lex/B upper limit. In all models the Lex/B count rate predicted is at least one order of magnitude higher than the upper limit. We have therefore concluded that the detection of RT Lac in Al/Ti/C is most likely to be spurious.

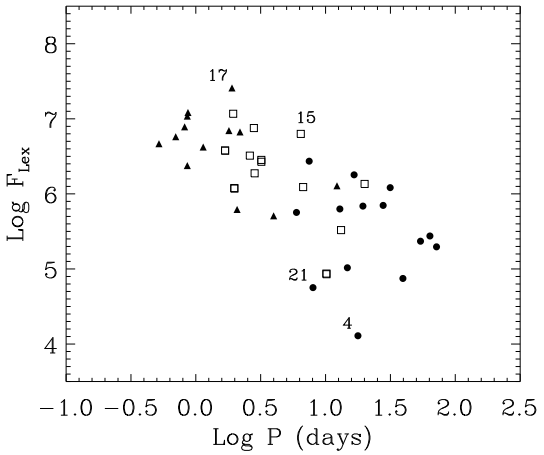

Fig. 8. The log–log diagram of surface Lex/B flux in erg cm^{-2} s^{-1} against photometric period (days). Symbols as in Fig. 2.

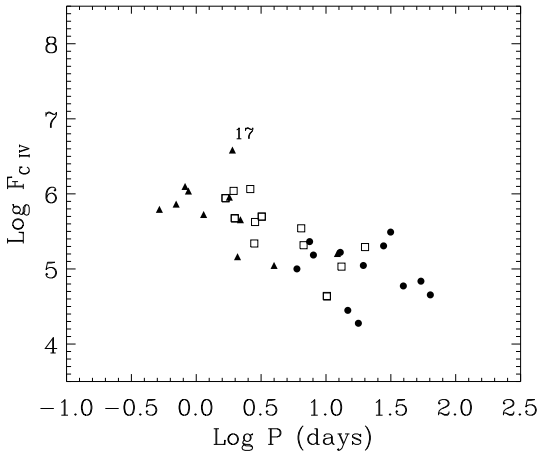

Fig. 9. The log–log diagram of surface CIV flux in erg cm^{-2} s^{-1} against photometric period; Symbols as in Fig. 2.

6. Conclusions

A search of Extreme Ultraviolet Explorer all-sky survey data for 104 RS CVn systems resulted in 38 significant detections in the Lex/B passband and 11 in the Al/Ti/C; an increase of 40% over that previously found (if we consider the ROSAT WFC, the increase is 25%). Using single temperature coronal models the corresponding fluxes have been determined. A very good correlation exists between the CIV 1550Å flux and the Lex/B data. Using observed CIV fluxes, we have worked backways from our correlation verifying the observed EUVE upper limits for systems not detected by the EUVE satellite. By comparing the Lex/B radiated output to the X–ray we conclude that, for the RS CVn systems, the radiative losses in the EUV region of the spectrum represent a smaller fraction of the total radiative losses emerging from the stellar corona than they do in the case of active late–type stars. A general trend of increasing Lex/B flux (with a well defined upper limit and a leveling-off for the faster rotators among the dwarfs) with decreasing rotation is evident. Some of the brighter sources have being observed (e.g. Schrijver et al. 1995, Dupree et al. 1993) with the EUVE spectrometers, however as is evident from Table 1, several other sources are sufficiently bright to enable good quality spectra of individual spectral lines to be obtained.

Acknowledgements. We wish to thank the EUVE principal investigators Drs. S.Bowyer and R.F.Malina for their advice and support. Research at Armagh Observatory is grant–aided by the Dept. of Education for N. Ireland,s while partial support for software and hardware is provided by the STARLINK Project which is funded by the UK PPARC. MM acknowledges support from a Royal Society grant to Queens University of Belfast and NASA grant NAS5-30180 while working at Berkeley. We are grateful to Dr. Antonella Fruscione for providing us with the interstellar column densities. We wish to thank Jeneen Sommers & Ken Anderson for their help during CKM visit to Berkeley. This research has made use of the Simbad database, operated at CDS, Strasbourg, France. Part of this work was also funded by a grant to Armagh Observatory and the University of Athens from the British Council and the Greek Ministry of Industry, Research and Technology. We also wish to thank the anonymous referee for his perceptive comments and remarks.

References

Ayres T.R., 1984, ApJ 284, 784
Basri G., Laurent R. & Walter F.M., 1985, ApJ 298, 761
Bowyer S., Lieu R., Lampton M., Lewis J., Wu X., Drake J.J. & Malina R.F., 1994, ApJSS 93, 569 (BSC)
Bruner M.E. & McWhirter R.W.P., 1988, ApJ 326, 1002
Dempsey R.C., Linsky J.L., Schmitt J.H.M.M.& Fleming T.A., 1993a, ApJ 413, 333
Dempsey R.C., Linsky J.L., Fleming T.A. & Schmitt J.H.M.M., 1993b, ApJSS 86, 599
Doyle J.G., Mitrou C.K., Mathioudakis M. & Antonopoulou E., 1994, A&A 283, 522
Doyle J.G., 1996, A&A 307, 162
Drake S.A., Simon T. & Linsky J.L., 1989, ApJSS, 71, 905
Dupree A.K., Brickhouse N.S., Doschek G.A., et al, 1993, ApJ 418, L41
Fox D.C., Linsky J.L, Veale A., et al, 1994, A&A 284, 91
Fruscione A., Hawkins I., Jelinsky P. & Wiercigroch A., 1994, ApJSS 94, 127
Fruscione A., 1996, ApJ 459, 509
Gurzadyan G.A. & Rustambekyan S.S., 1994, ApSS 211, 171
Jelinsky P. & Fruscione A., 1996, (in preparation)
Katsova M.M. & Tsikoudi V., 1993, ApJ 402, L9
McGale P.A., Pye J.P., Barber C.R. & Page C.G., 1996, MNRAS 275, 1232
Malina R.F., Marshall H.L., Behram A., et al, 1994, AJ 107 (2), 751 (BSL)
Mathioudakis M., Fruscione A., Drake J.J., McDonald K., Bowyer S. & Malina R.F., 1995, A&A 300, 775
Mitrou C.K., Doyle J.G., Mathioudakis M. & Antonopoulou E., 1996, 'Proc of the 9th Workshop on Cool Stars, Stellar Systems and the Sun'
Monsignori-Fossi B., Landini M., 1994, Solar Physics 152, 81
Patterer R.J., Vedder P.W., Jelinsky P., Brown A. & Bowyer S., 1993, ApJ 414, L57

Pounds K.A., Allan D.J., Barber C. et al., 1993, MNRAS 260, 77
Pye J.P., McGale P.A., Allan D.J., et al, 1996, MNRAS 275, 1165 (2RESC)
Rumph T., Bowyer S. & Vennes S., 1994, AJ 107, 2108
Schrijver C.J., Mewe R., Van den Oord, G.H.J. & Kaastra J.S., 1995, A&A 302, 438
Simon T. & Fekel F.C, 1987, ApJ 316, 434
Strassmeier K.G., Hall D.S., Zeilik M., Nelson E., Eker Z. & Fekel F.C., 1988, A&AS 72, 291 (CCABS)
Strassmeier K.G., Hall D.S., Fekel F.C. & Scheck M., 1993, A&AS 100, 73 (2nd CCABS)

This article was processed by the author using Springer-Verlag LaTeX A&A style file *L-AA* version 3.